CHAPTER 2 REVIEW OF RELEVANT STUDIES

An investigation into the seismic behavior of an innovative structural system, BRKB-TMF was conducted in this research. This system combines features from three different systems including a truss moment frame, a knee braced moment frame and a buckling restrained braced frame. In this research, BRKB-TMF was designed by a powerful performance-based plastic design (PBPD) method. Collapse assessment was performed according to FEMA P695 methodology (FEMA, 2009). Relevant studies regarding the structural systems, the design methodology and the performance evaluation method are briefly reviewed in the following sections.

2.1 Truss Moment Frames

Open-web steel truss girder frames are an economical structural system commonly used for building structures, especially industrial and low-rise ones. Their advantages over solid web beams and girders include:

- Light weight, especially for large spans
- Simple connections to columns.
- Large passages for mechanical ductwork and pipes

However, under extreme loading events, conventional truss girders may lack proper ductility which often causes sudden and catastrophic failures. This disadvantage is caused by buckling of the elements due to compressive forces. A half-span subassemblage test of open-web truss moment frame was performed by Goel and Itani (1994a). The test setup and the experimental result are illustrated in Figures 2.1 and 2.2, respectively. The test result indicated that after the lateral force was applied until the lateral displacement reached 50 mm, the strength and stiffness suddenly dropped because the force in one of the diagonal members reached its axial compression capacity and the members buckled.

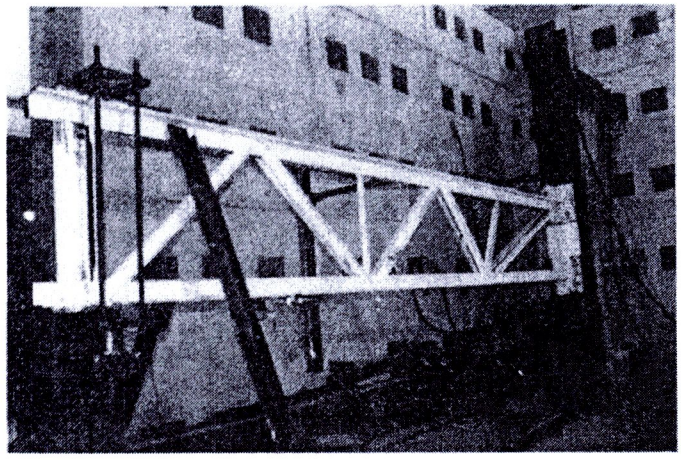

Figure 2.1 Test Setup (Goel and Itani, 1994a)

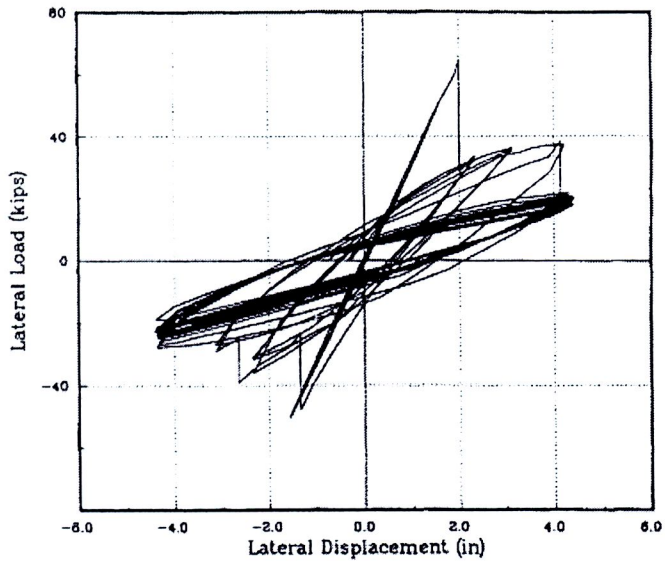

Figure 2.2 Hysteretic Loop of Conventional Open-Web Truss Moment Frame tested by Goel and Itani (1994a)

Based on results of the experiment, Special Truss Moment Frame (STMF) system was developed in order to enhance the inelastic deformation capacity. This system is currently recognized as a valid seismic resistant system in the AISC seismic provisions (AISC, 2010b). This system uses ductile segments to dissipate seismic energy. Columns and truss segments outside the special segments are designed to remain elastic under the forces generated by fully yielded and strain-hardened special segments. The test result of a STMF subassemblage illustrated in Figure 2.3 indicates that hysteretic characteristic of this system is stable and no longer affected by buckling of the members as intended by the design concept of STMF.

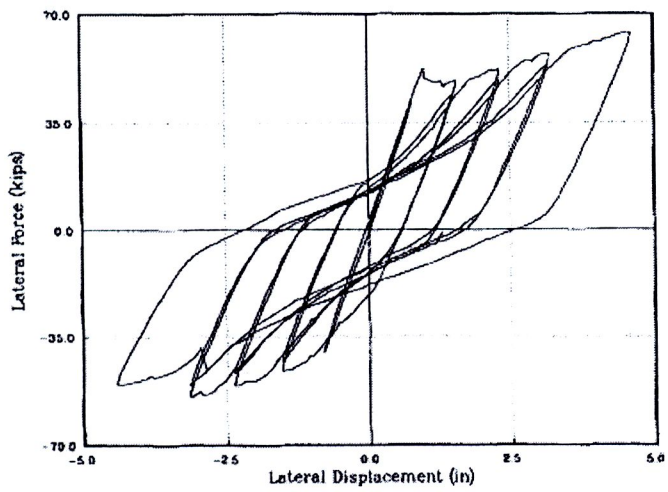

Figure 2.3 Hysteretic Loop of Special Truss Moment Frame tested by Goel and Itani (1994b)

In this research, the performance of STMF system is further enhanced by using a buckling restrained brace (BRB). The yielding is confined to the BRBs and the trusses are designed to be entirely elastic. This result in a better repairability of the system since the BRBs can be easily replaced after a severe earthquake.

2.2 Knee Braced Moment Frames

The effectiveness of knee bracing was investigated by Leelataviwat et al. (2011). In the study, knee braced moment frame (KBMF) system was proposed. A KBMF is a structural system that combines the features of eccentrically braced frames and moment frames. Pre-selected mechanism of this hybrid system is that, under severe seismic event, knee braces will yield and buckle followed by plastic hinging of a beam at the ends of the beam segment outside the knee portions as illustrated in Figure 2.4. Test results indicate that hysteretic characteristic of the KBMF is ductile and stable as illustrated in Figure 2.5.

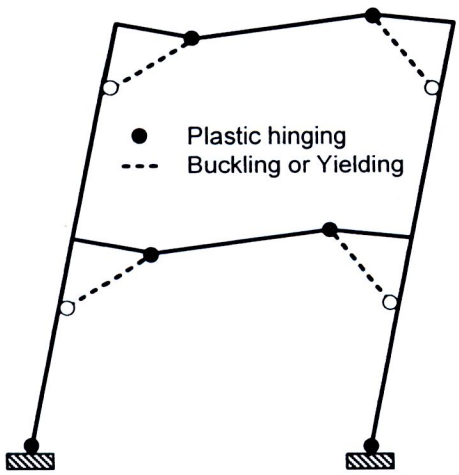

Figure 2.4 Yield Mechanism of KBMF System (Leelataviwat et al., 2011)

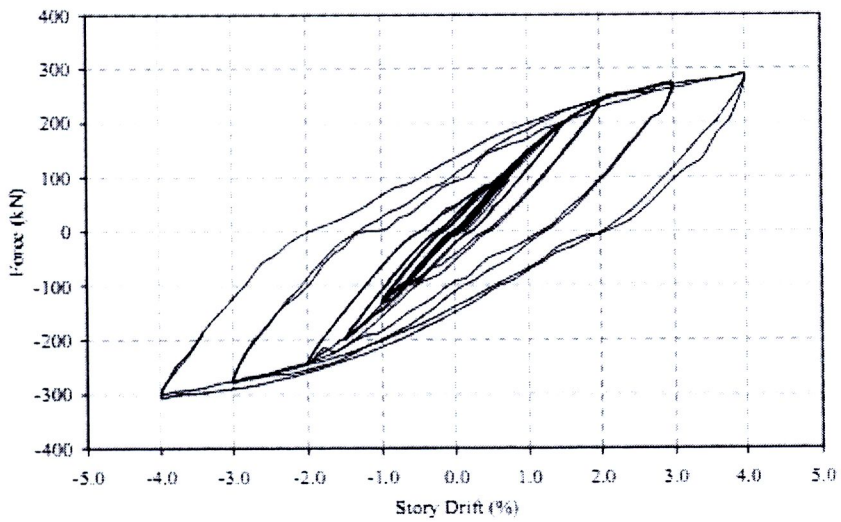

Figure 2.5 Hysteretic Response of KBMF (Leelataviwat et al., 2011)

The results also indicate that knee braces actively take part in resisting seismic load. When properly designed, knee braces can yield in tension and compression, and can dissipate significant seismic energy.

2.3 Buckling Restrained Braces (BRBs)

In the structural system proposed in this study, buckling restrained braces (BRBs) are used as knee braces. BRBs are now widely used to resist seismic forces. They have stable hysteretic behavior unlike conventional steel braces. BRBs are widely used in concentrically brace frames. Its application is usually found in a V- or a inverted V-braced (chevron) configuration. In tension, the brace yields, while in compression, buckling is restricted by a restraining mechanism. Therefore, BRBs are able to achieve ductile yielding in both tension and compression.

A number of different BRB configurations have been developed (Bozorgnia and Bertero, 2004). A typical BRB consists of two main components: steel core and casing. A typical BRB configuration is illustrated in Figure 2.6. The steel core is made of a rectangular plate which is responsible for resisting the applied load. The core is wrapped with a thin layer of a debonding material and is inserted in to a casing. The casing is typically constructed of a mortar filled steel tube that mainly aims to prevent the core from buckling. A typical hysteretic response of a BRB is also shown in Figure 2.6.

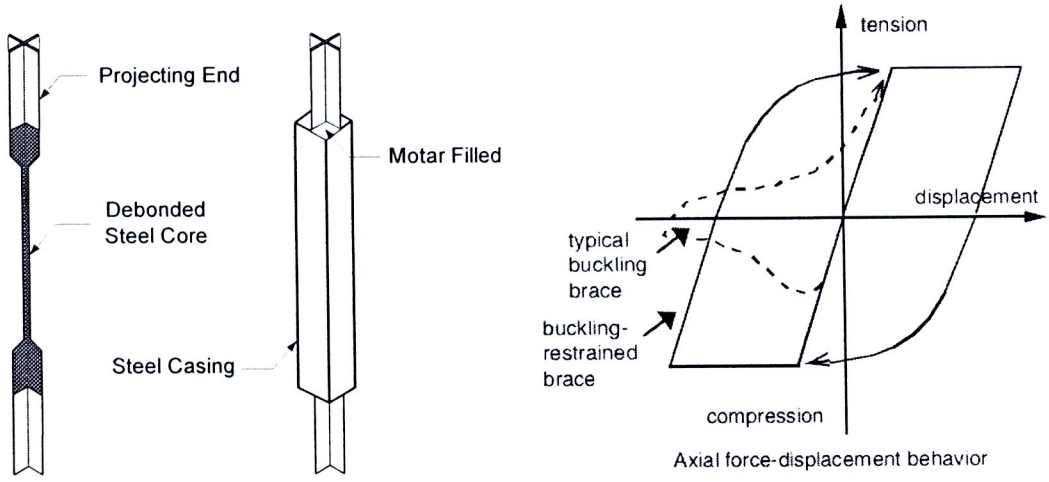

Figure 2.6 Behavior of BRB compared with that of a Conventional Brace (Clark et al., 1999)

A large numbers of experiments have been carried out on BRBs. Lopez and Sabelli (2004) summarized selected test results performed during 1999 and 2003. The summary is shown in Table 2.1 along with recent test results performed at King Mongkut's University of Technology Thonburi (Ngamsangeam, 2010). The tests were typically done with two test types, uniaxial and subassemblage. The brace sizes and length varied in the tests. Hysteretic loops of an example BRB (Merritt et. al, 2003b) is illustrated in Figure 2.7. As can be seen, its response is full and ductile.

Table 2.1 BRB Tests Results Summarized by Lopez and Sabelli (2004), and those by Ngamsangeam (2010)

Literature Reference	Test Type	Core Material	Length (m)	Max. Brace Strain (%)
SIE, 1999	Uniaxial	JIS G3136 SM 490A	4.50	2.07
			4.50	2.07
			4.50	2.07
SIE, 2001	Uniaxial	JIS G3136 SN 400B	4.50	2.07
			4.50	2.07
UC Berkeley, 2002	Frame (Subassemblage)	JIS G3136 SN 400B	3.00	2.12
			4.72	1.88
			4.72	1.81
Merritt et al., 2003a	Subassemblage	ASTM A36	5.50	2.50
			5.50	2.50
			5.50	2.68
			5.50	2.62
			5.50	2.48
			5.80	2.40
Merritt et al., 2003b	Subassemblage	ASTM A36	6.40	2.43
			6.40	2.48
			6.40	1.84
			6.40	2.47
			6.40	2.64
			6.40	2.54
			6.40	1.84
			6.40	1.77
Merritt et al., 2003c	Uniaxial	ASTM A36	6.10	1.60
			6.10	1.72
SIE, 2003	Subassemblage	JIS G3136 SN 400B	4.22	2.73
			4.22	2.96
			7.55	1.64
			7.55	1.63
Ngamsangeam, 2010	Uniaxial	ASTM A36	0.85	1.37
			0.85	1.83
			0.85	1.83
			0.85	1.83
			0.90	2.75
			0.90	1.83
	Subassemblage	ASTM A36	1.60	1.50

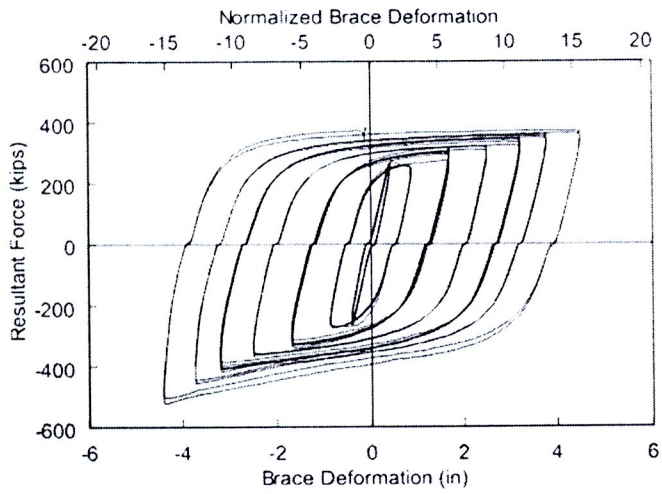

Figure 2.7 Hysteretic Response of BRBs (Merritt et al, 2003b)

From the test results, it can be seen that BRBs are able to deform up to a strain level of approximately 2.6%. In terms of core strain, this strain capacity is approximatly 3.7%. The maximum core strain is a very important parameter in the design of the proposed BRKB-TMF system. In the proposed system, the structure relies solely on the BRBs to dissipate seismic energy. Therefore, the design must ensure that the deformation of BRBs will not exceed the strain capacity under the design basis earthquake level and under the maximum considered earthquake level. This can be done using the performance-based plastic design procedure as presented in the following section. The relationship between the maximum core strain and the design target drift as well as the effect of the ductility of the BRBs (as expressed by the maximum core strain) on the overall response of BRKB-TMF will be further explored in Chapter 6.

2.4 Performance-Based Plastic Design (PBPD)

PBPD method is based on the plastic analysis at yield state (mechanism). The PBPD method uses a pre-selected target drift and a yield mechanism as key performance limit states. These two limit states are directly related to the degree and distribution of structural damage, respectively. The design base shear for a specified hazard level is calculated by equating the work needed to push the structure monotonically up to the target drift to the energy required by an equivalent EP-SDOF to achieve the same state. Plastic design is then performed to obtain details of the frame members and connections that will provide the intended yield mechanism and behavior.

The advantages of the mechanism-based PBPD approach as mentioned above include:

- The deformation of key structural members can be controlled. This results in enhanced performance and safety, especially under severe ground motions.
- The frame can be repaired with relative ease after a seismic event because the structural damage (yielding) would be confined to known yielding members (referred to as Designated Yielding Members, DYM) and locations.
- Other members which are not designed to yield (referred to as non-Designated Yielding Members, non-DYM) would not need to be detailed for stringent ductility requirements.

- Innovative structural schemes can be developed by selecting an appropriate yield mechanism and a variety of ductile energy dissipating members. This reason is why PBPD is selected and applied in this research.

In the PBPD method, energy balance (Lee and Goel, 2001) is used to equate energy from monotonic load-deformation response of the inelastic system with the corresponding elastic system, as illustrated in Figure 2.8. The energy balance equation as proposed by Lee and Goel (2001) is given by:

$$\gamma E = \gamma \frac{1}{2} M S_v^2 = E_e + E_p \tag{2-1}$$

where E_e and E_p are the elastic and plastic components of the energy needed to push the structure up to the target drift, respectively, S_v is the design pseudo-spectral velocity, M is the total mass of the system, and γ is the energy factor (Lee and Goel, 2001). The energy factor is defined as the ratio of the energy absorbed by the inelastic system to that of the equivalent elastic system and is given by:

$$\gamma = \frac{2\mu_s - 1}{R_\mu^2} \tag{2-2}$$

where μ_s is the ductility ratio and R_μ is the yield force reduction factor (V_e/V). The energy factor can be computed for a given ductility using an R_μ-μ-T relationship such as the one developed by Newmark and Hall (1982). For seismic design purposes, a target ductility level can be selected and the energy factor can be computed.

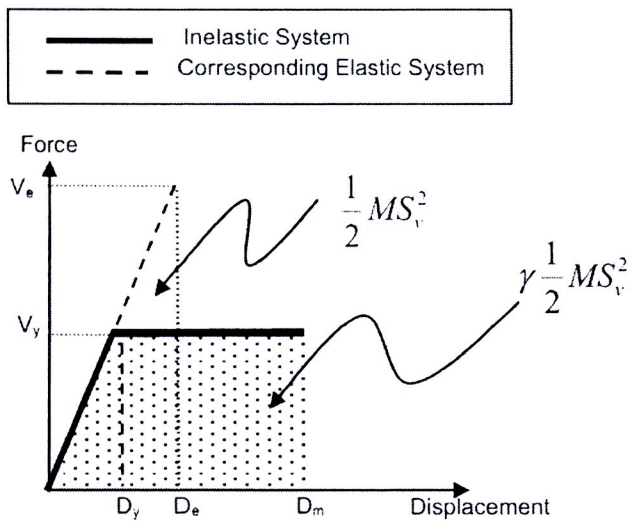

Figure 2.8 Energy Balance Concept (Lee and Goel, 2001)

By using an appropriate lateral force distribution along the height of the frame and using the selected mechanism, the E_e and E_p components in Equation 2-1 can be evaluated. The required base shear strength (V) of the system (Lee and Goel, 2001) can be determined as follows:

$$\frac{V}{W} = \frac{-\alpha + \sqrt{\alpha^2 - 4\gamma C_e^2}}{2} \tag{2-3}$$

where W is the weight of the structure, C_e is normalized design pseudo acceleration (S_a/g) and α is a parameter given by:

$$\alpha = \left(\sum_{j=1}^{n} \lambda_i h_i\right) \frac{\theta_p 8\pi^2}{T^2 g} \tag{2-4}$$

where θ_p is the target plastic story drift, T is the period, and h_i is the height from the ground to floor level i, and λ_i is the lateral force distribution factor. The lateral force at level i is assumed to be of the form:

$$F_i = \lambda_i V \tag{2-5}$$

In general, the lateral force distribution should closely represent an actual pattern that occurs under earthquake ground motions. Because of the lack of available data for BRKB-TMF, a distribution based on the inelastic response of steel MRF systems (Chao et al., 2007) is used in this study and is given by:

$$\lambda_i = (\beta_i - \beta_{i+1}) \left(\frac{w_n h_n}{\sum_{j=1}^{n} w_j h_j} \right)^{0.75T^{-0.2}} \tag{2-6}$$

where w_n is the weight of the structure at the top level n, h_n are the heights from the ground to the top level, and β_i is a ratio of the story shear at level i to that of the top story (level n).

$$\beta_i = \frac{V_i}{V} = \left(\frac{\sum_{j=1}^{n} w_j h_j}{w_n h_n} \right)^{0.75T^{-0.2}} \tag{2-7}$$

Once the lateral forces have been determined, the frame can be designed using plastic analysis. The PBPD procedure for BRKB-TMF system will be discussed in detail in Chapter 3.

2.5 Performance Assessment per FEMA P695 Methodology

In this research, the assessment of the seismic performance of BRKB-TMF was carried out based on FEMA P695 methodology. FEMA P695 is an alternative methodology for structural building assessment. The performance evaluation is based on a probabilistic analysis and collapse margin calculation to assess the expected structural safety. FEMA P695 is based on the incremental dynamic analysis (IDA) approach (Vamvatsikos and Cornell, 2002). The collapse of structure is determined by monotonically increase ground motion intensity until the structure reaches the collapse point. Cumulative distribution function (CDF) is used to present probability of collapse by means of a fragility curve (Ibarra et al., 2002). In FEMA P695 methodology, sources of uncertainty such as record-to-record, availability of test data, design requirement, and modelling quality are included in the analysis.

Response of a structure according to FEMA P695 methodology is illustrated in Figure 2.9. It is defined in the form of a relationship between a spectral acceleration and lateral deformation. In current design practice, reduction of ground motion intensity at maximum considered earthquake level (S_{MT}) to design level (C_s) is used in a design process. Consequently, the structure behaves inelastically when subjected to an earthquake ground motion, and reaches the critical deformation at the collapse level ground motion (S_{CT}) as illustrated in Figure 2.9. Collapse margin ratio (CMR) is defined as the ratio between the median spectral acceleration of the collapse level ground motions and the spectral acceleration at the MCE level:

$$CMR = \frac{SD_{CT}}{SD_{MT}} = \frac{S_{CT}}{S_{MT}} \tag{2-8}$$

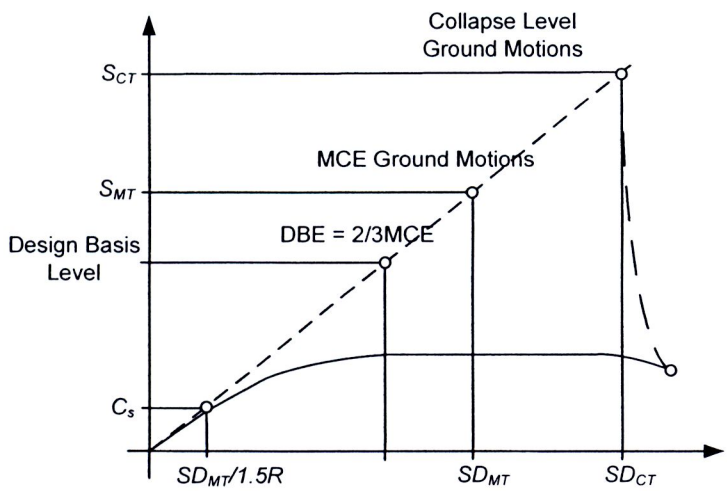

Figure 2.9 Collapse Assessment Concept of FEMA P695 Methodology

IDA approach is used to determine S_{CT} by performing nonlinear time history analyses with a record set (44 far-field ground motions) as recommended in the methodology. The ground motions are listed in Table 2.2. Two components of each ground motion are used in the analyses. Figure 2.10 shows the response spectra of the ground motions with the median spectral acceleration at the period of 1 sec. scaled to 0.96g (MCE level).

Table 2.2 Summary of Far-Field Record Set

Earthquake			PEER-NGA Record Information			Recorded Motions	
Name	Year	M	Record No.	Component 1	Component 2	PGAmax (g)	PGVmax (cm/s)
Northridge	1994	6.7	953	NORTHR/MUL009	NORTHR/MUL279	0.52	63
Northridge	1994	6.7	960	NORTHR/LOS000	NORTHR/LOS270	0.48	45
Duzce, Turkey	1999	7.1	1602	DUZCE/BOL000	DUZCE/BOL090	0.82	62
Hector Mine	1999	7.1	1787	HECTOR/HEC000	HECTOR/HEC090	0.34	42
Imperial Valley	1979	6.5	169	IMPVALL/H-DLT262	IMPVALL/H-DLT352	0.35	33
Imperial Valley	1979	6.5	174	IMPVALL/H-E11140	IMPVALL/H-E11230	0.38	42
Kobe, Japan	1995	6.9	1111	KOBE/NIS000	KOBE/NIS090	0.51	37
Kobe, Japan	1995	6.9	1116	KOBE/SHI000	KOBE/SHI090	0.24	38
Kocaeli, Turkey	1999	7.5	1158	KOCAELI/DZC180	KOCAELI/DZC270	0.36	59
Kocaeli, Turkey	1999	7.5	1148	KOCAELI/ARC000	KOCAELI/ARC090	0.22	40
Landers	1992	7.3	900	LANDERS/YER270	LANDERS/YER360	0.24	52
Landers	1992	7.3	848	LANDERS/CLW-LN	LANDERS/CLW-TR	0.42	42
Loma Prieta	1989	6.9	752	LOMAP/CAP000	LOMAP/CAP090	0.53	35
Loma Prieta	1989	6.9	767	LOMAP/G03000	LOMAP/G03090	0.56	45
Manjil, Iran	1990	7.4	1633	MANJIL/ABBAR--L	MANJIL/ABBAR--T	0.51	54
Superstition Hills	1987	6.5	721	SUPERST/B-ICC000	SUPERST/B-ICC090	0.36	46
Superstition Hills	1987	6.5	725	SUPERST/B-POE270	SUPERST/B-POE360	0.45	36
Cape Mendocino	1992	7	829	CAPEMEND/RIO270	CAPEMEND/RIO360	0.55	44
Chi-Chi, Taiwan	1999	7.6	1244	CHICHI/CHY101-E	CHICHI/CHY101-N	0.44	115
Chi-Chi, Taiwan	1999	7.6	1485	CHICHI/TCU045-E	CHICHI/TCU045-N	0.51	39
San Fernando	1971	6.6	68	SFERN/PEL090	SFERN/PEL180	0.21	19
Friuli, Italy	1976	6.5	125	FRIULI/A-TMZ000	FRIULI/ATMZ270	0.35	31

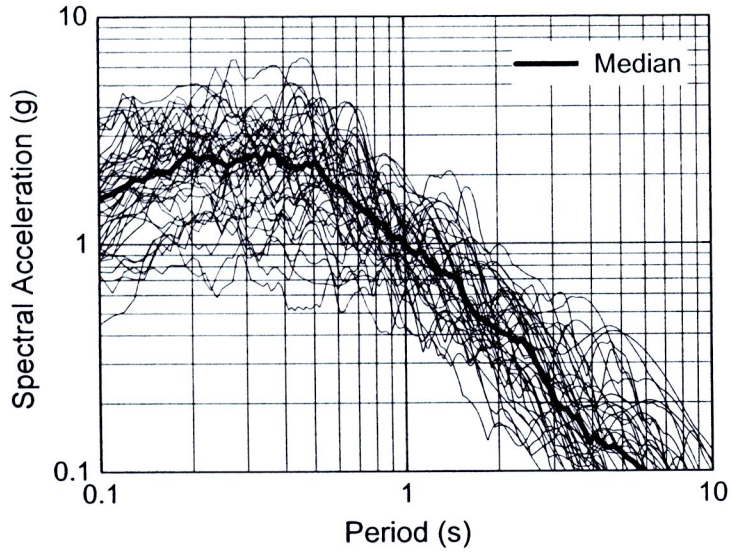

Figure 2.10 Response Spectra of 44 Individual Components of the Normalized Far-Field Record Set and Median

The analyses were performed by incrementally scaling up the ground motions until the structure instability or collapse occurs. Figure 2.11 shows an example of the analysis results under one ground motion. The IDA results are presented by a plot of the median spectral acceleration values at the fundamental period of the structure occurs to maximum interstory drifts. The results of a record set are presented as illustrated in Figure 2.12. Each curve in the figure represents the results for an individual ground motion. When the curve approaches horizontal level, large lateral deformation and, consequently, structural instability or collapse occurs. S_{CT} and S_{MT} can then be determined from the results.

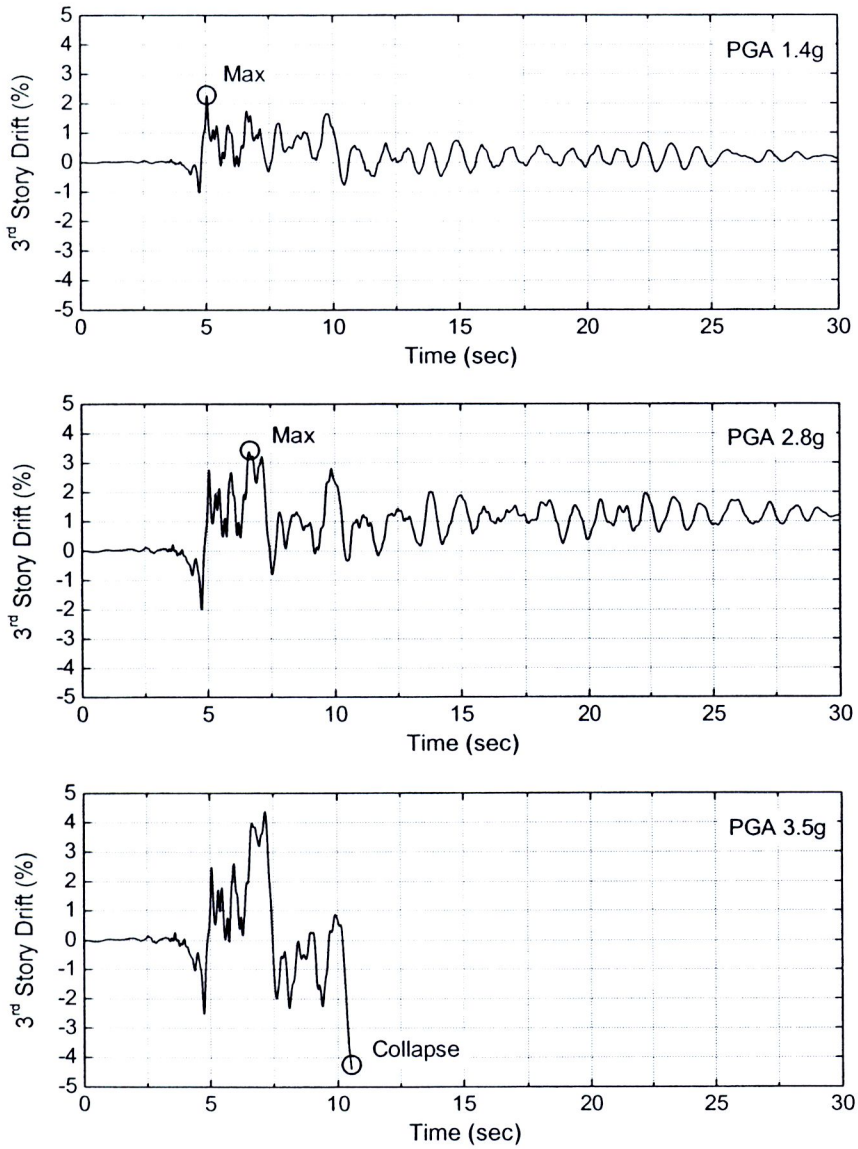

Figure 2.11 Example of Response under a Selected Ground Motion with Increasing Intensity

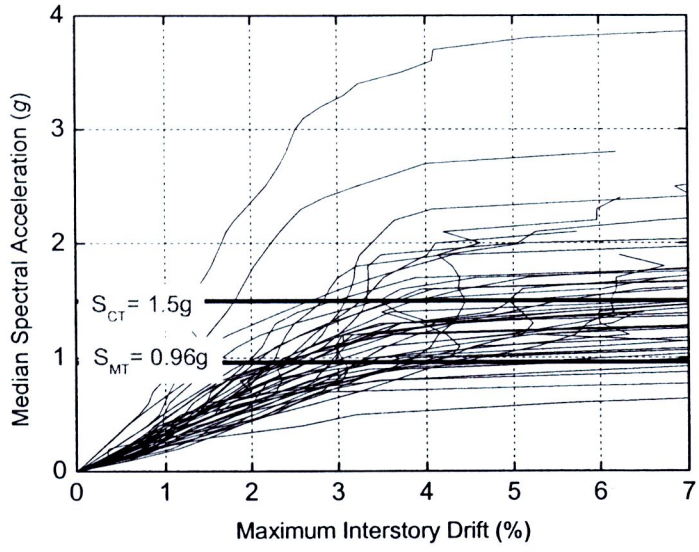

Figure 2.12 Dynamic Response of the Structure by IDA Approach

Instead of using the relationship between median spectral acceleration values and maximum interstory drifts, IDA results can be presented in terms of the probability of collapse by a fragility curve as illustrated in Figure 2.13. Probability of collapse at any given intensity level can be computed from the ratio of number of ground motions that cause collapse to the total number of ground motions used in the analysis.

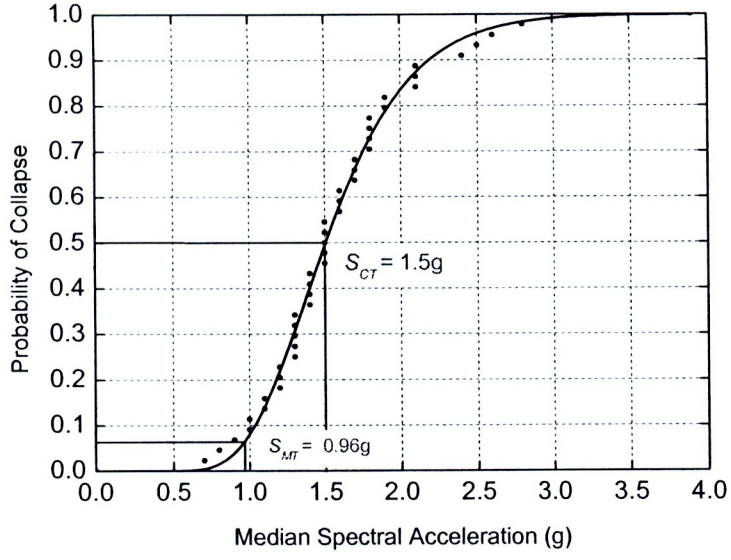

Figure 2.13 Fragility Curve of an Example Archetype Structure

S_{CT} is the median spectral acceleration value in which half of the ground motion causes collapse (ratio of the number of ground motions that cause collapse to the total number of ground motions equals to 0.5, or 50 percent chance of collapse).

Variation of ground motion records, ground motion record scaling, difference between the characteristics of the response spectra of actual ground motions and the design spectrum, and adequacy of test data can all influence the collapse margin ratio value (*CMR*). In order to determine an accurate *CMR* value, all sources of uncertainties must be taken into account.

FEMA P695 methodology accounts for the spectral shape effect (Baker and Cornell, 2006) in collapse margin calculation by using a spectral shape factor (*SSF*). The *CMR* value is multiplied by *SSF* to obtain the adjusted collapse margin ratio as shown:

$$ACMR = SSF \times CMR \tag{2-9}$$

where *ACMR* is the adjusted collapse margin ratio. The spectral shape factor depends on the period-based ductility (μ_T) value, the overstrength of the structure, and the fundamental period (Baker and Cornell, 2006; FEMA, 2009). Nonlinear static analyse (pushover) is performed to obtain the overstrength factor (Ω) and the period-based ductility value (μ_T). These two parameters are used to determine *SSF* to account for spectral shape effect. An example of *SSF* values for different values of the fundamental period and period-based ductility (μ_T) for seismic design category D_{max} are listed in Table 2.3.

Table 2.3 Spectral Shape Factor for Archetype for SDC D_{max} on Example Range

T (sec.)	Period-Based Ductility (μ_T)							
	1.0	**1.1**	**1.5**	**2**	**3**	**4**	**6**	**≥8**
0.8	1.00	1.06	1.12	1.16	1.22	1.27	1.35	1.41
0.9	1.00	1.06	1.13	1.17	1.24	1.29	1.37	1.44
1.0	1.00	1.07	1.13	1.18	1.25	1.31	1.39	1.46
1.1	1.00	1.07	1.14	1.19	1.27	1.32	1.41	1.49
1.2	1.00	1.07	1.15	1.2	1.28	1.34	1.44	1.42

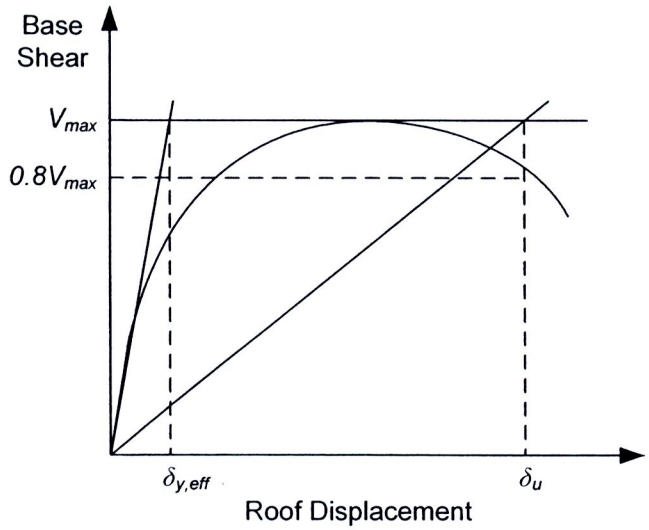

Figure 2.14 Idealized Nonlinear Static Pushover Curve (FEMA, 2009)

An idealized pushover curve is illustrated in Figure 2.14. The overstrength factor is defined as the ratio of the maximum base shear (V_{max}) to the design base shear (V) as:

$$\Omega = \frac{V_{max}}{V} \tag{2-10}$$

The period-based ductility (μ_T) is defined as the ratio of ultimate roof drift displacement (δ_u) to the effective yield roof drift displacement ($\delta_{y,eff}$) as:

$$\mu_T = \frac{\delta_u}{\delta_{y,eff}} \tag{2-11}$$

The ultimate roof drift displacement is taken as the roof drift when the base shear equals 80% of V_{max}. The effective yield roof drift is given by the following formula:

$$\delta_{y,eff} = C_0 \frac{V_{max}}{W}\left[\frac{g}{4\pi^2}\right]\left(\max\left(T, T_1\right)\right)^2 \tag{2-12}$$

where C_0 relates fundamental-mode (SDOF) displacement to the roof displacement, V_{max}/W is the maximum base shear normalized by building weight, g is the gravitational constant, T is the fundamental period computed as $C_u T_a$, C_u is given in ASCE 7 and the approximate fundamental period T_a is based on a regression analysis of actual building data (Chopra et at., 1998), and T_1 is the fundamental period of the archetype model computed using eigenvalue analysis.

In the evaluation, the performance is deemed to be acceptable when the adjusted collapse margin ratio of the structure exceeds the minimum required *ACMR* value. According to FEMA P695, the minimum *ACMR* value is defined as $ACMR_{10\%}$ when a group of structures is considered and $ACMR_{20\%}$ when an individual structure is considered.

For a group of structures, the performance is deemed to be acceptable when the average value of the adjusted collapse margin ratio (*ACMR)* of each performance group exceeds $ACMR_{10\%}$ or:

$$\overline{ACMR} \geq ACMR_{10\%} \tag{2-13}$$

For an individual structure, the performance is deemed to be acceptable when each individual *ACMR* ratio ($ACMR_i$) of each structure in group exceeds $ACMR_{20\%}$ or:

$$ACMR_i \geq ACMR_{20\%} \tag{2-14}$$

$ACMR_{10\%}$ and $ACMR_{20\%}$ limits depend on total system collapse uncertainty (β_{TOT}), including record-to-record variation, design requirements, adequacy of test data, and modelling uncertainty. The total system collapse uncertainty (β_{TOT}) is determined by rating record-to-record, design requirements, test data and modelling uncertainties as superior, good, fair, or poor rank. An example of values of total system collapse uncertainty (β_{TOT}) for good modelling quality and period-based ductility greater than 3

are listed in Table 2.4. Once β_{TOT} has been determined, $ACMR_{10\%}$ and $ACMR_{20\%}$ can be found. An example of $ACMR_{10\%}$ and $ACMR_{20\%}$ values for different values of β_{TOT} are listed in Table 2.5.

Table 2.4 Total System Collapse Uncertainty Value (β_{TOT}) for Model Quality Good (B) and Period-Based Ductility, $\mu_T \geq 3$

Quality of Test Data	Quality of Design Requirements			
	(A) Superior	(B) Good	(C) Fair	(D) Poor
(A) Superior	0.475	0.500	0.575	0.675
(B) Good	0.500	0.525	0.600	0.700
(C) Fair	0.575	0.600	0.675	0.750
(D) Poor	0.675	0.700	0.750	0.825

Table 2.5 Acceptable Values of Adjusted Collapse Margin Ratio on Example Range

Total System Collapse Uncertainty (β_{TOT})	Collapse Probability	
	10% ($ACMR_{10\%}$)	20% ($ACMR_{20\%}$)
0.525	1.96	1.56
0.550	2.02	1.59
0.575	2.09	1.62
0.600	2.16	1.66
0.625	2.23	1.69